A wide Chandra view of the core of the Perseus cluster

Andy C. Fabian, Jeremy S. Sanders, S. W. Allen, R. E. A. Canning, E. Churazov, C. S. Crawford, William R. Forman, J. Gabany, J. Hlavacek-Larrondo, Roderick M. Johnstone, et al.

Monthly Notices
of the
ROYAL ASTRONOMICAL SOCIETY

Mon. Not. R. Astron. Soc. **418,** 2154–2164 (2011) doi:10.1111/j.1365-2966.2011.19402.x

A wide *Chandra* view of the core of the Perseus cluster

A. C. Fabian,[1⋆] J. S. Sanders,[1] S. W. Allen,[2,3] R. E. A. Canning,[1] E. Churazov,[4] C. S. Crawford,[1] W. Forman,[5] J. GaBany,[6] J. Hlavacek-Larrondo,[1] R. M. Johnstone,[1] H. R. Russell,[7] C. S. Reynolds,[8] P. Salomé,[9] G. B. Taylor[10⋆] and A. J. Young[11]

[1]*Institute of Astronomy, Madingley Road, Cambridge CB3 0HA*
[2]*Kavli Institute for Particle Astrophysics and Cosmology, Department of Physics, Stanford University, 452 Lomita Mall, Stanford, CA 94305-4085*
[3]*SLAC National Accelerator Laboratory, 2575 Sand Hill Road, Menlo Park, CA 94025, USA*
[4]*Max-Planck-Institut for Astrophysics, Karl-Schwarzschild-str. 1, 85741 Garching, Germany*
[5]*Harvard–Smithsonian Center for Astrophysics, 60 Garden St., Cambridge, MA 02138, USA*
[6]*Blackbird 2 Observatory, Alder Springs, CA 93602, USA*
[7]*Department of Physics and Astronomy, University of Waterloo, ON N2L 3G1, Canada*
[8]*Department of Astronomy, University of Maryland, College Park, MD 20742, USA*
[9]*LERMA, Observatoire de Paris, UMR 8112 du CNRS, 75014 Paris, France*
[10]*Department of Physics and Astronomy, University of New Mexico, Albuquerque, NM 87131, USA*
[11]*H. H. Wills Physics Laboratory, University of Bristol, Tyndall Avenue, Bristol BS8 3HG*

Accepted 2011 July 7. Received 2011 July 5; in original form 2011 May 24

ABSTRACT

We present new *Chandra* images of the X-ray emission from the core of the Perseus cluster of galaxies. The total observation time is now 1.4 Ms. New depressions in X-ray surface brightness are discovered to the north of NGC 1275, which we interpret as old rising bubbles. They imply that bubbles are long-lived and do not readily breakup when rising in the hot cluster atmosphere. The existence of a 300 kpc long NNW–SSW bubble axis means there cannot be significant transverse large-scale flows exceeding 100 km s^{-1}. Interesting spatial correlations are seen along that axis in early deep radio maps. A semicircular cold front about 100 kpc west of the nucleus is seen. It separates an inner disturbed region dominated by the activity of the active nucleus of NGC 1275 from the outer region where a subcluster merger dominates.

Key words: galaxies: clusters: general – galaxies: individual: NGC 1275 – intergalactic medium – X-rays: galaxies.

1 INTRODUCTION

New large-scale *Chandra* data on the core of the Perseus cluster, A 426, are presented here. They follow our earlier 900 ks ACIS-S image which covered an 8 × 8 arcmin region centred on the nucleus of the dominant galaxy NGC 1275 (Fabian et al. 2000, 2006; Sanders & Fabian 2007). That image, with hints from neighbouring CCD chips, indicated that bubbles, filaments and other fine-scale structure extended over a wider field. The new data extend the area imaged in detail to a region over 30 × 15 arcmin^2. *XMM* observations of the Perseus cluster, of lower spatial resolution but covering an even wider area than that discussed here, have been presented and discussed by Churazov et al. (2003).

The Perseus cluster is the X-ray brightest cluster in the sky (Forman et al. 1972), having peaked emission first resolved with the *Copernicus* satellite (Fabian et al. 1974). Einstein X-ray imaging showed a dip in the X-ray emission to the north-west (NW) of the nucleus of the central galaxy, NGC 1275 (Branduardi-Raymont et al. 1981; Fabian et al. 1981). *ROSAT* High Resolution Imager data (Böhringer et al. 1993) showed that this dip was an outer bubble in the hot X-ray-emitting gas and resolved two inner bubbles coincident with the Fanaroff–Riley type I radio source, 3C84 (Pedlar et al. 1990). Churazov et al. (2000) showed that the bubbles are inflated by the radio jets and rise buoyantly in the surrounding hot gas. The NW bubble was formed a few 10^7 yr ago and is now moving outwards. Estimates of the likely energies and time-scales indicated the power in the bubbling process to be of the order of 10^{45} erg s^{-1}. *Chandra* images resolve the bubbles in detail (Fabian et al. 2000) and show subtle ripples centred on the inner bubbles which are interpreted as weak shocks or sound waves produced by the bubbles (Fabian et al. 2003a). The shape of the NW bubble resembles the cross-section of a rising spherical cap bubble in water on the Earth (Fabian et al. 2003b), despite being over 10^{22} times larger. Rising bubbles drag out cooler X-ray-emitting gas (as in the Virgo cluster; Churazov et al. 2001) from the centre and cold gas (the Hα filaments of NGC 1275; Lynds 1970; Conselice, Gallagher & Wyse 2001; Fabian et al. 2003b, 2008).

⋆E-mail: acf@ast.cam.ac.uk (ACF); gbtaylor@unm.edu (GBT)

In this paper we present evidence for further structures along the bubbling axis which may be older, outer bubbles or merged bubbles.

The cluster is assumed to have a redshift of 0.0183, corresponding to an angular scale of 0.37 kpc arcsec^{-1} ($H_0 = 70$ km s^{-1} Mpc^{-1}).

2 THE NEW IMAGES

The new ACIS-I images have been mosaicked together into a single image (0.5–7 keV, shown in Fig. 1). The average at each radius has been subtracted for display purposes. The central structure is associated with the bubbles formed by the radio jets from the active nucleus and is detailed in our earlier work. The separate ACIS-I chips are 16 × 16 arcmin and the whole image is 35.5 arcmin from north to south (788 kpc).

We have added the earlier 900-ks ACIS-S images to make the final composite (Fig. 2). The nucleus of most member galaxies of the Perseus cluster are detected (see Santra, Sanders & Fabian 2007). The point source in the image to the WSW of the nucleus of NGC 1275 (about halfway to the edge) corresponds to the nucleus of the optically second-brightest cluster galaxy, NGC 1272 (see Fig. 3). It sits on a rim of X-ray bright cluster emission. This rim is seen as a step at 6–7 arcmin radius from the nucleus of NGC 1275 in Figs 4, 5 and 6, and is roughly circular in shape with a centre displaced 1 arcmin to the NW of that nucleus. We return to the large-scale structure to the west in Section 6.

Fig. 3 (right) was produced with the 0.5-m telescope at the Blackbird Observatory, located in the south central Sacramento Mountains of New Mexico, USA. The image represents over 31 h of cumulative exposure time through broad-band clear, red, green, blue and 6 nm narrow-band filters. Each subexposure was reduced following standard procedures for bias correction and flat-fielding. Master dark and bias frames were created by combining 10 dark subexposures, each produced at the same exposure length and camera temperature settings used for the luminance and the filtered images. A master flat was produced by combining 10 separate sky-flat exposures for each filter. The clear, red, green, blue and 6 nm narrow-band filtered exposures were separately combined (using a median procedure) to produce individual master data sets. Each master data set was then projected into a grey-scale image, intensity scaled, assigned to its appropriate primary colour and then digitally combined with the other data sets to produce a full colour picture. The 6 nm narrow-band data set was used to supplement the intensity of the red broad-band colour channel; the clear data set was used to intensify luminance information for the combined data sets. Post-processing methods that resulted with the final image followed standard procedures that are also employed to create Hubble Heritage images (Rector et al. 2007).

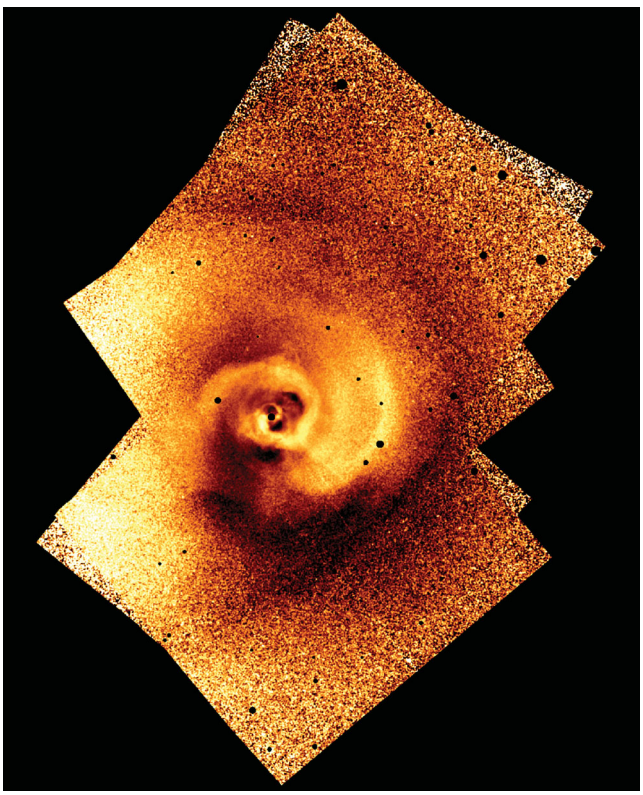

Figure 1. Mosaic of new images only, exposure corrected and adaptively smoothed. The light streaks to the south-west (SW) direction are due to the CCD readout of the bright nucleus of NGC 1275 and have no effect on the conclusions of this paper. The separate ACIS-I pointings are evident, each has a side of 16 arcmin.

3 NEW STRUCTURES

Overlays of the new composite X-ray image with the Hα filaments around NGC 1275 and deep radio data at 49 cm (Sijbring 1993) are shown in Figs 7 and 8. As noted by Fabian et al. (2006), there is a loop-like X-ray structure at the end of the long northern Hα filament. This could be a fallback of the outer parts of the cooler gas dragged out to the north by earlier bubbles, when the optical filament was created.

Further structures to the north are then expected and indeed observed. The radio image shows an extension at the end of the optical filament above which there is a spur leading to a dark patch in the X-ray image, corresponding to a drop in flux, which we call the northern trough. [Burns et al. (1994) published a deep 330 MHz Very Large Array radio image of Perseus which shows similar outer structure, lending credence to the details being real.] Just to the west of the radio spur lie two elliptical-shaped dips in the X-ray image which we identify as old outer bubbles. The outer of these was found originally on an outer chip of the deepest ACIS-S observations (Sanders & Fabian 2007). These structures are indicated in Fig. 9 and shown in profile in Fig. 10.

A bay is seen to the SSE of NGC 1275 (Fabian et al. 2006), along the bubble axis (Figs 8 and 9). The radio contours indicate a coincident minimum in radio flux.

3.1 The northern trough and bubbles

The northern trough (structure labelled A in Fig. 6) lies 9 arcmin (200 kpc) north of the nucleus . We have studied it through profiles made by spectral analysis along a sector to the north (Fig. 11). It is about 10 per cent deep in surface brightness and likely lies along, or close to, an equipotential. It is also along the main jet axis to the north where within the inner 40 kpc or so there is a pronounced optical Hα filament (Figs 3 and 7). If such a filament has been dragged out by rising large bubbles (see Fabian et al. 2003b; Hatch et al. 2006), then it is plausible that the trough could be the remains of those bubbles.[1]

[1] The possibility that the jet has changed direction or precessed is discussed by Dunn, Fabian & Sanders (2006). The mean axis over the past $\sim 5 \times 10^8$ yr remains along the NNW–SSW direction.

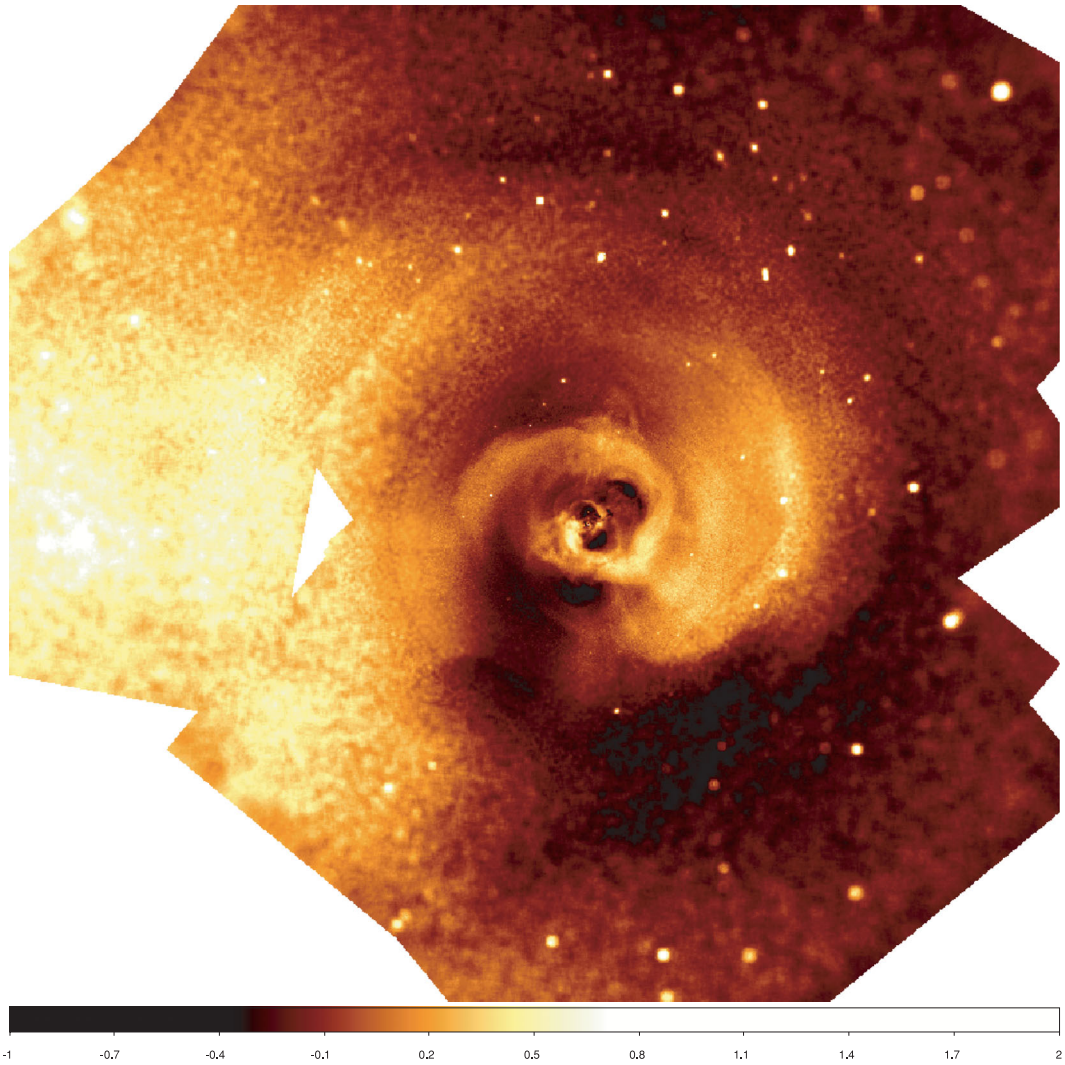

Figure 2. Final composite image of the 1.4-Ms exposure in the 0.5–7 keV band, adaptively smoothed with a kernel with a fixed number of counts (225 in each of three energy bands, which have then been summed) and with the average at each radius subtracted. The colour shows fractional variation. The image is 25.6 arcmin from north to south. The optically second-brightest galaxy in the cluster, NGC 1272, lies along the bright rim 5 arcmin (111 kpc) west of the nucleus. There is no coverage of a small triangular region to the east of NGC 1275.

We can start to explore a bubble origin by comparing the volume of the trough with that of one of the observed bubbles near the centre. A rough estimate of the volume of the trough can be made assuming that it is an ellipsoid with its major axis, of length 2.5 arcmin, i.e. 55 kpc, in the plane of the sky and radius 0.7 arcmin, i.e. 15.5 kpc. This provides a 10 per cent dip in surface brightness, as observed, if the integrated depth along the line of sight is equivalent to the central value multiplied by the radius from the nucleus. This volume is about 5.6×10^4 kpc^3, or about 21.5 times that of the inner north bubble, which has a radius of 8.5 kpc.

The external pressure drops by a factor of 3 between the centre and 10-arcmin radius where the trough resides (Fig. 11), which is a pressure of about $n_e T_e \sim 7 \times 10^5$ K cm^{-3} . Adiabatic expansion then gives a factor of about 2 increase in volume, so we are looking at the accumulation of about 11 bubbles similar to the present inner ones (assuming the contents are preserved during the rise). The energy content of the trough is $4PV = 1.2 \times 10^{60}$ erg. This is one and two orders of magnitude smaller than the events that have occurred in the Hydra A (Nulsen et al. 2005) and MS 0735.6+7421 (McNamara et al. 2009) clusters, respectively.

The possibility that the trough represents the accumulation of the last 500 Myr or so of bubbles arises (a similar structure is discussed for A2204 by Sanders, Fabian & Taylor 2009). Bubbles rise and are trapped at some radius, in this case at about 220 kpc. Perhaps, they become neutrally buoyant there due to mixing with surrounding gas, or the magnetic structure (possibly azimuthal there; Quataert et al. 2008) traps them. There also seems to be an overall structure at and just within that radius to the west, possibly due to motion of the core relative to the outer cluster gas (see e.g. Churazov et al. 2003).

The two X-ray surface brightness dips to the SW of the trough (Figs 9 and 10), which we identify as rising bubbles, have volumes of approximately 10^4 kpc^3 each, corresponding to about twice that of the current inner bubbles.

The bay to the south may result from the accumulation of southward rising bubbles in analogy to the northern trough. It has a sharp, curved northern edge and the interior is hotter than the outer parts (Fig. 12). Perhaps, there has been some mixing and heating taking place between the relativistic and thermal intracluster gases. It lies much closer to the nucleus of NGC 1275.

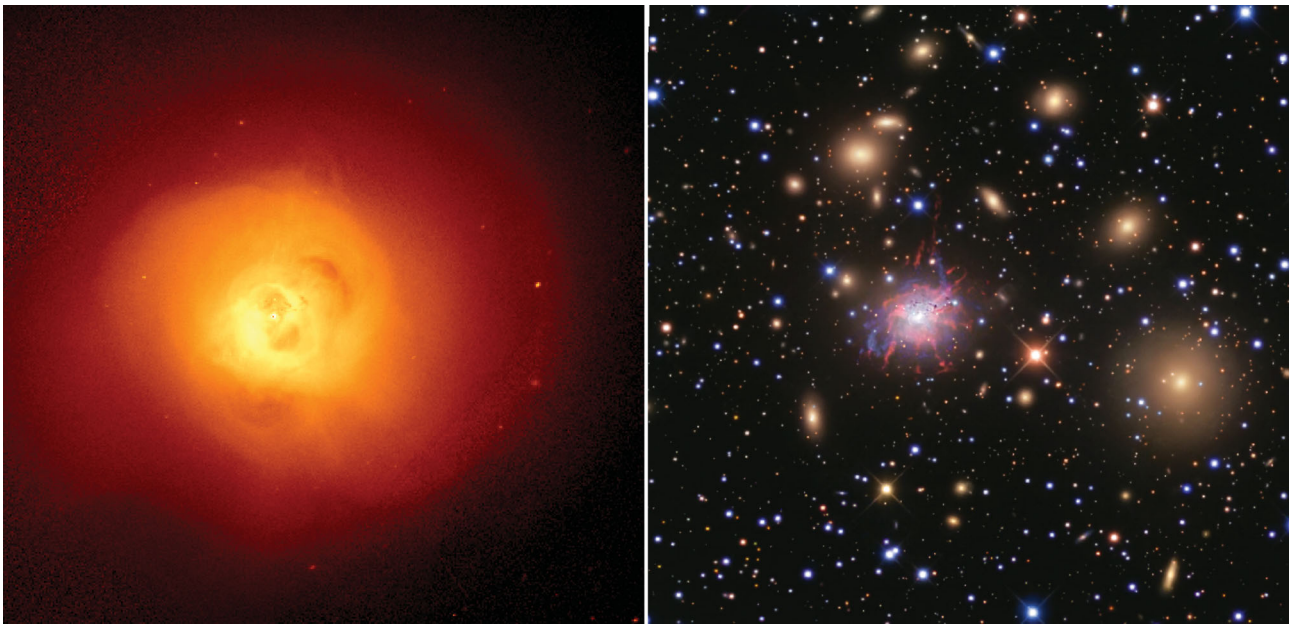

Figure 3. Matching X-ray and optical images of the core of the Perseus cluster. Left: *Chandra* composite (from Fig. 2, but without subtraction of the mean at each radius). Right: optical from Blackbird Observatory (see text for details). The images are 11.8 arcmin from north to south. NGC 1272 is the bright elliptical galaxy 5 arcmin WSW of NGC 1275.

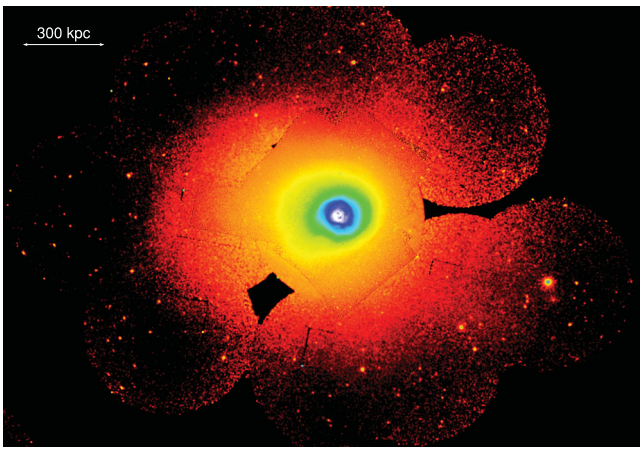

Figure 4. Joint *Chandra* and *XMM* image.

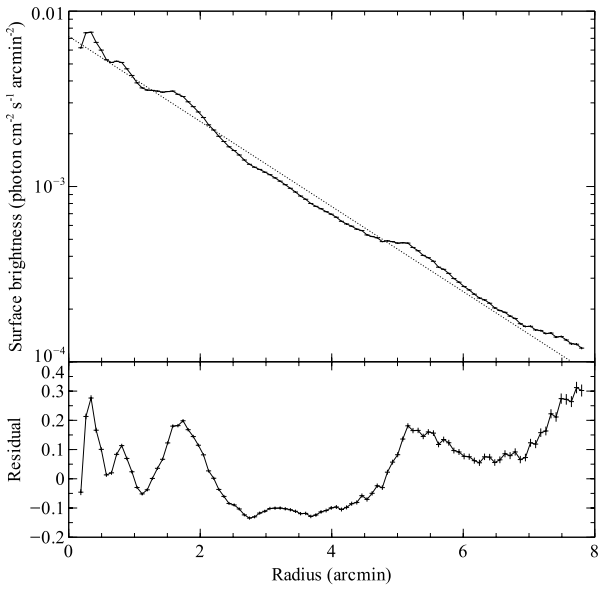

Figure 5. Surface brightness profile in the 0.5–7 keV band to the west of the nucleus of NGC 1275.

The evolution of rising bubbles in cluster gas has been studied and simulated by many authors (e.g. Diehl et al. 2008; Liu et al. 2008). Bubbles blown by a jet are not Rayleigh–Taylor unstable because the upper surface of the bubble is not at rest relative to the hot gas above them. The expansion of the bubbles means that the hot gas continuously flows around them. The growth time of the Kelvin–Helmholtz instability is comparable to the flow time. Whether they breakup or not depends on the amplitude and scale of velocity perturbations in the hot gas. The stability of a large gas bubble rising through liquid has been studied by Batchelor (1987). Rising air bubbles in water can be surprisingly large. The scale size of disruptive perturbations depends on surface tension (which in the case of cluster bubbles means magnetic field), viscosity and gravitational acceleration. Lyutikov (2006) has proposed that magnetic draping can provide a surface tension. Reynolds et al. (2005) have discussed and simulated the role of viscosity in rising bubbles. Higher viscosity leads to stable, long-lived, bubbles.

Diehl et al. (2008) show that the bubbles seen at larger radii in several clusters tend to be much larger than those at smaller radii, larger even than expected by adiabatic expansion. In Hydra A, where three pairs of expanding bubbles are identified (Wise et al. 2007), there is a progressive steep increase of bubble radius with distance from the nucleus (see also Randall et al. 2011, for a sequence of bubbles in an elliptical galaxy).

Diehl et al. (2008) discuss bubbles which are continuously fed energy from the nucleus, which seems unlikely for Perseus. We note that if the rising speed of a bubble depends on its size and if a merger always occurs if two bubbles meet, then a sequence of bubbles of slightly varying size will at larger radii become a set of

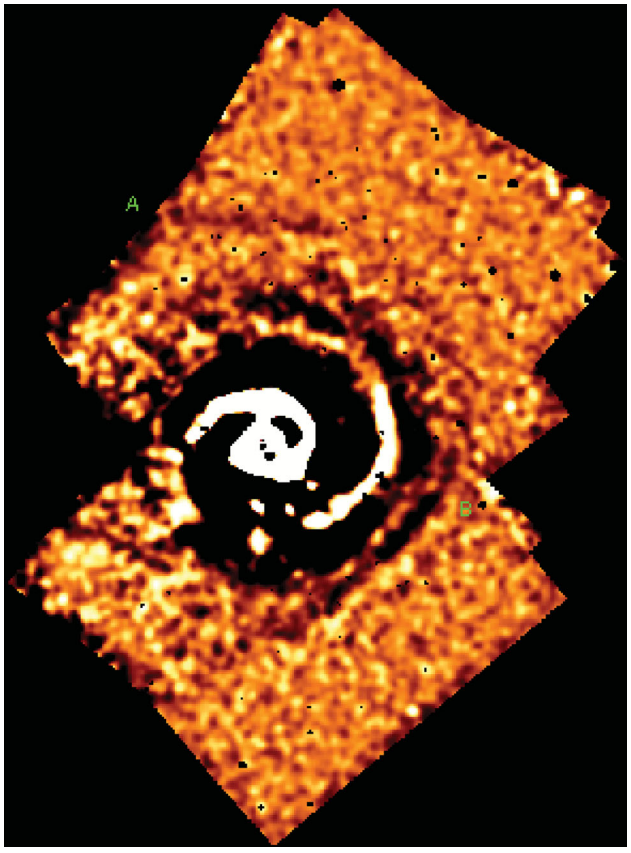

Figure 6. Unsharp masked image using larger regions than for Fig. 1.

fewer larger bubbles. The radius at which this happens will depend on the steepness of the bubble size–speed relation and the initial size variation amplitude. It will happen if both larger ones are faster or slower. This could well explain our observations of the outer Perseus bubbles.

It is not clear what is happening to the south of the nucleus. The early observations showed an inner and an outer bubble there. At larger radii there is a sharp edge to part of an elliptical-shaped structure which we term the bay. This could represent the end point for bubbles rising in that direction. The temperature there (Fig. 12) is hotter. This could either be because there is hotter gas at that radius, or because relativistic plasma has displaced gas and we are only seeing the projected outer hotter intracluster gas. The pseudo-pressure maps (Figs 13 and 14) do, however, peak in this region, so the first option is preferred. The energy in this cavity, assuming it contains only thermal gas and a prolate-ellipsoidal shape, is 1.7×10^{60} erg, slightly more than for the northern trough.

4 TEMPERATURES, PRESSURES AND METALS

The new data have been contour-binned (Sanders 2006) into regions each with 22 500 counts (signal-to-noise ratio of 150). The spectra within each bin have been fitted separately resulting in the temperature and metallicity maps shown in Fig. 13. [The Anders & Grevesse (1989) abundance table has been used.] The higher metallicity gas does stretch to the north in the direction of the trough, but no more detailed correspondence is evident. We also show a pseudo-pressure map (obtained from the square root of the mean surface brightness in each region multiplied by the temperature).

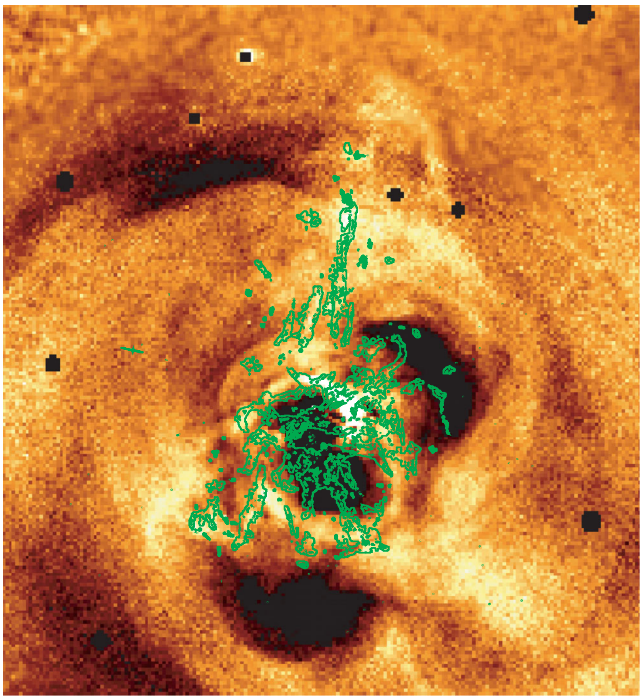

Figure 7. Inner part of the X-ray image with Hα contours (from Conselice et al. 2001) overlaid. The image is 6.8 arcmin (150 kpc) from north to south.

A semicircular cold front is seen to the west. Across this front the temperature jumps from 5.5–6 to 7–8 keV, and the metallicity drops from 0.55–0.6 to 0.4–0.45. The pressure declines relatively smoothly across the region (see also Figs A1 and A2 in Appendix A). The smooth pressure change while the temperature jumps is characteristic of a cold front (see Section 6 for further discussion).

Finally, Fig. 14 shows the temperature and pseudo-pressure maps obtained when the mean value at that radius (from the nucleus of NGC 1275) has been subtracted, to highlight small differences.

5 RADIO CORRELATIONS

Minihaloes such as 3C84 are rare (Ferrari et al. 2008) and may be due to turbulence (Gitti et al. 2004). There is a possible association between minihaloes and gas sloshing (ZuHone, Markevitch & Brunetti 2011) in cluster cores (Mazzotta & Giacintucci 2008). The swirl seen in the temperature maps is indicative of gas sloshing, perhaps induced by an off-axis merger or at least the close passage of a stripped group core (Churazov et al. 2003; Ascasibar & Markevitch 2006; Roediger et al. 2011).

We have noted interesting correlations between structures in the radio and X-ray maps (Fig. 8). While there might be small-scale turbulence in the hot gas, we doubt that there is considerable hydrodynamic turbulence due to the straightness and ordered structures of the Hα filaments. Indeed, the 40–50 kpc long northern filament shows little evidence for turbulent flow.

The large-scale linearity of the bubble structures shown in Fig. 8, apart from the northern trough, is evidence against significant large-scale flows or rotation of the core gas. If we conservatively take a minimum transverse motion of 50 kpc (the semimajor axis of the trough) over the time to make the structures, say 5×10^8 yr, we obtain a maximum transverse velocity of 100 km s^{-1}. (The time estimate here is the buoyancy rise time of the outermost bubbles using the expression of Churazov et al. 2001.)

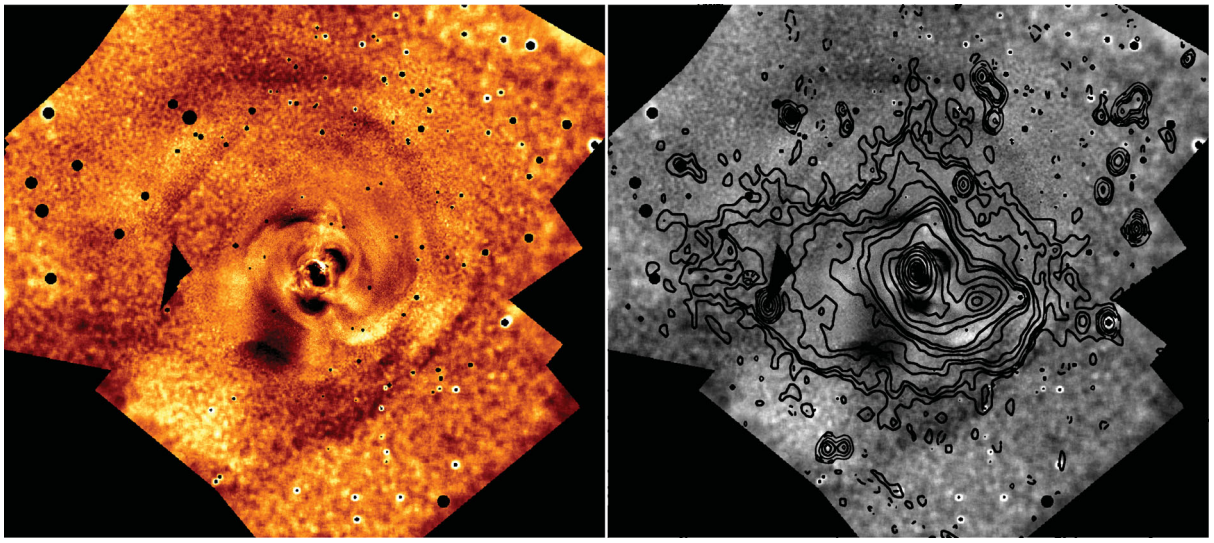

Figure 8. Left: *Chandra* X-ray image residuals obtained after subtracting a smooth elliptical model. Ellipses were fitted to surface brightness contours, and an elliptical model created by interpolating between these ellipses. Right: radio contours (from Sijbring 1993) overlaid on the X-ray image. The radio data of 3C84 were taken at 49 cm (608.5 MHz). Similar structures are seen in the 92-cm map. The radio contours stop abruptly at the edge of the outer ring of X-ray emission to the SW. A spur of radio emission to the north points towards the trough.

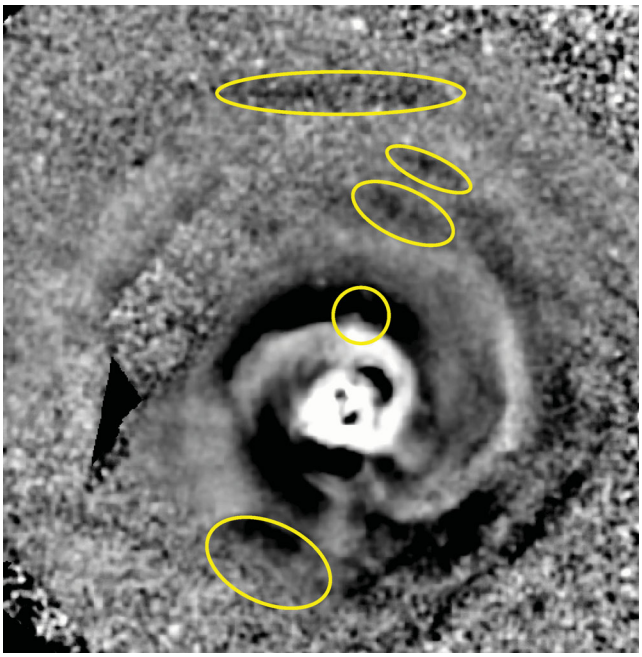

Figure 9. Structures identified in the composite image; from top to bottom – northern trough, two older rising bubbles, top of north Hα filament and south 'bay' (old bubble?).

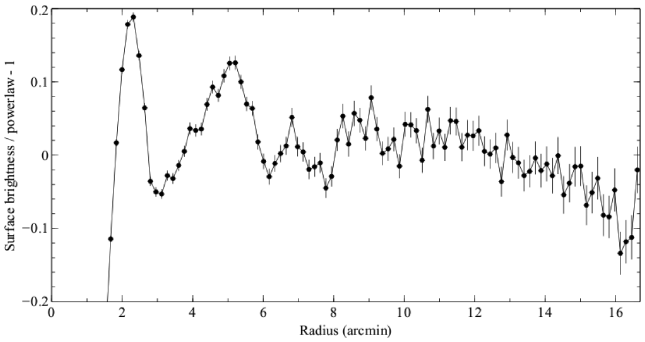

Figure 10. Surface brightness profile to the NNW. The dips at ∼6 and 7.7 arcmin are the two northernmost bubbles.

6 LARGE-SCALE STRUCTURES AND COLD FRONTS

The western edge, rim and semicircular structure seen in Figs 1,2,5 and 6 appears to separate the inner active galactic nuclei (AGN) dominated region from the outer cluster. As outlined in Section 4, the temperature rises sharply to the west of the structure, whereas the pseudo-pressure shows no abrupt change (Figs 13–15 and A1). It therefore appears to be a cold front (for a review see Markevitch & Vikhlinin 2007), and is probably related to a past subcluster merger (Churazov et al. 2003; Section 5).

Mergers producing slopping/sloshing/bathtub/seich modes in the core of the Perseus cluster have been discussed for decades (see e.g. Allen et al. 1992), since Einstein Observatory imaging showed the overall emission to be lopsided (Branduardi-Raymont et al. 1981). Such modes can persist for a considerable time (Gyr). Cold fronts can form in the process (e.g. Birnboim, Keshet & Herquist 2010). Tangential flows below the front and magnetic fields amplification are expected (Keshet et al. 2010). Once again we note the lack of evidence for significant transverse flows in the relatively straight Hα filament system or indeed in the NNW–SSW bubble axis, so any cold front flows do not penetrate far. Radial velocity measurements of the Hα filaments show smooth laminar flow (Hatch et al. 2006; Salomé et al. 2011).The radio minihalo does end abruptly at the front. The metallicity also undergoes a sharp change (Fig. 13).

The Perseus cluster will be an excellent target for high-resolution X-ray spectroscopy, such as anticipated with *Astro-H* (Takahashi et al. 2010). This will resolve the velocities flows along the line of sight. Both the central region where the bubbles form (Heinz, Brüggen & Morsony 2010) and the west cold front will be of great interest.

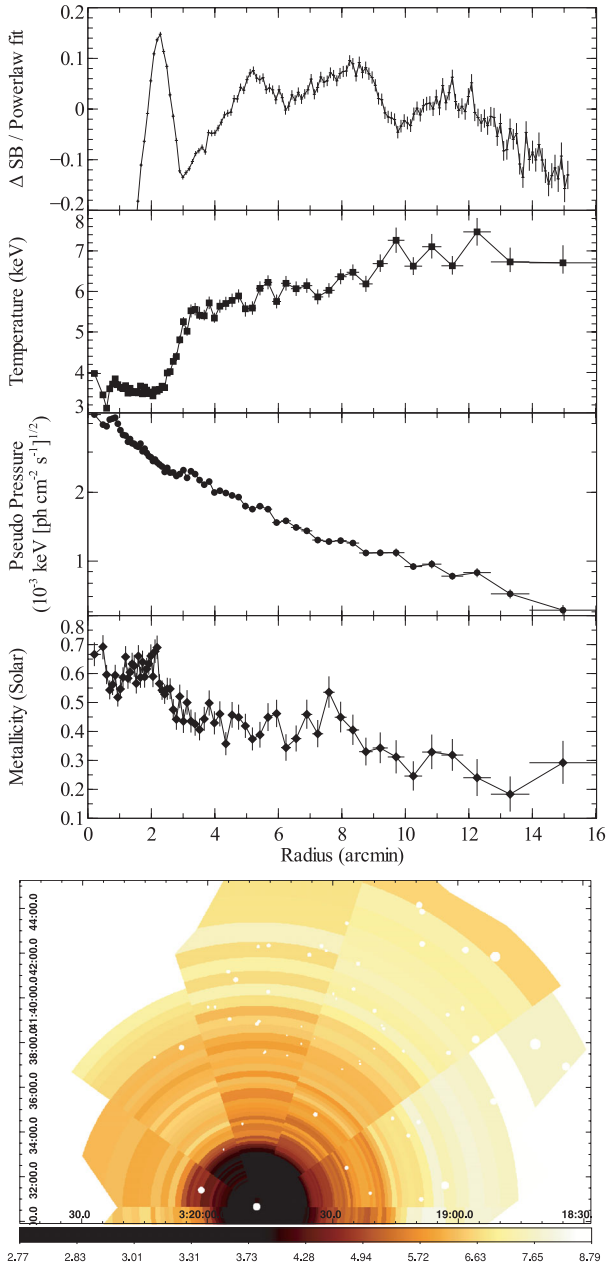

Figure 11. Profiles of differential surface brightness, temperature, pseudo-pressure and metallicity in the sector directly to the north (shown below).

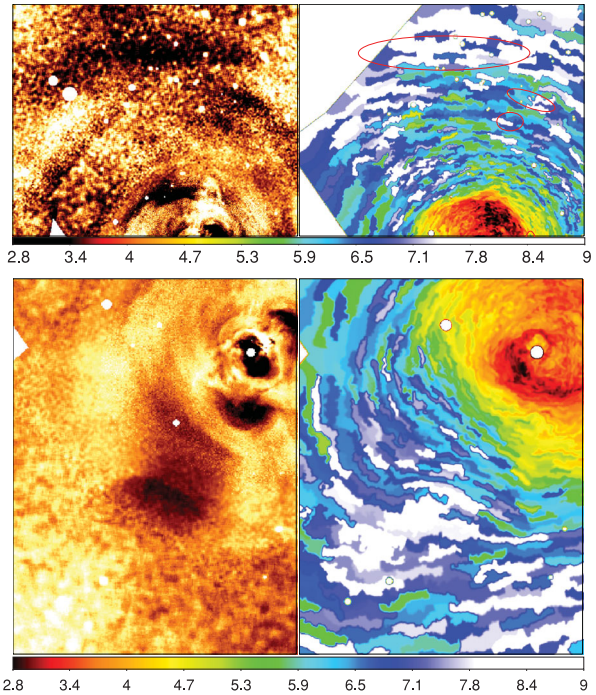

Figure 12. Top panel: surface brightness and temperature maps to the north. Lower temperature gas is seen stretching south to the centre of the northern trough. The two possible old bubbles coincide with higher temperature regions. The significance of this is not high since the temperatures have uncertainties of ∼0.5 keV). Lower panel: X-ray surface brightness with average at that radius subtracted (left) and temperature (right) to the south-east, showing the 'bay' which contains a 'tongue' of hotter material. A sharp cold front occurs around the northern side of the bay, but, being concave, is not a conventional cold front (Markevitch & Vikhlinin 2007).

6.1 The substructure profile

In order to assess the energy associated with large-scale structures in the Perseus cluster, we have characterized the energy/power needed to produce observed substructure (non-radial part) in the intracluster medium (ICM) (e.g. Fig. 6).

In order to cover a large radial range, we use *XMM–Newton* data. While not providing a high-resolution view on the Perseus core, they extend to larger radii than the existing *Chandra* data.[2] We first made a deprojection analysis of the data in four wedges (90° each), and for each wedge we calculated pressure in several radial shells spanning the range from few to 700 kpc. The thermal pressure nkT was evaluated in each radial bin, and rms variation of pressure between wedges was calculated as $\delta P = \langle [P - \langle P(r)\rangle]^2\rangle^{1/2}$. The ratio of this quantity to the mean pressure at the same radius $\frac{\delta P}{P} = \frac{\langle [P-\langle P(r)\rangle]^2\rangle^{1/2}}{P}$ can be used as a crude characteristic of the magnitude of the substructure (non-radial part) in the cluster. We then calculated the total thermal energy $E_{\rm th}(< r)$ of the ICM within a given radius as

$$E_{\rm th}(<r) = \int_0^r \frac{3}{2} nkT 4\pi r^2 \, {\rm d}r, \quad (1)$$

where n and T are the gas density and temperature at a given radius, and estimated the energy associated with the substructure $E_{\rm d}(< r)$ as

$$E_{\rm d}(<r) = \int_0^r \frac{3}{2} nkT \frac{\delta P}{P} 4\pi r^2 \, {\rm d}r. \quad (2)$$

The values of $E_{\rm th}(< r)$ and $E_{\rm d}(< r)$ and their ratio are plotted in the two bottom panels in Fig. 15. In the top panel the energy associated with substructure $E_{\rm d}(< r)$ is divided by the sound crossing time of the region $t_{\rm s} = r/c_{\rm s}$, where $c_{\rm s} = \sqrt{\gamma \frac{kT}{\mu m_{\rm p}}}$. The quantity

$$L_{\rm d} = \frac{E_{\rm d}(<r)}{t_{\rm s}} \quad (3)$$

can be regarded as an estimate of the power needed to maintain the observed non-radial substructure.

[2] Analysis of the *Chandra* data gives similar results over the 10–300 kpc range, but is noisier due to real structure at smaller radii and to photon noise at larger radii.

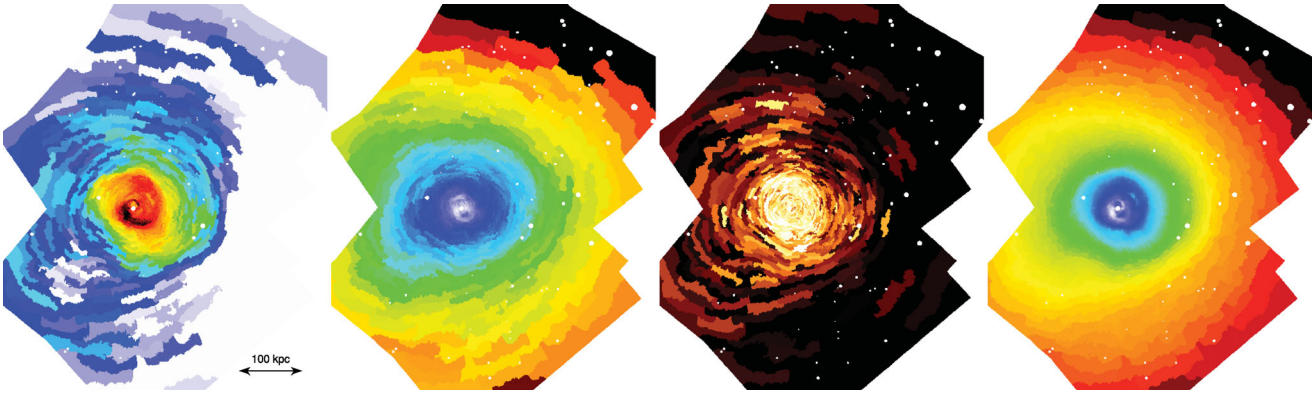

Figure 13. Distribution of (left to right) temperature, pseudo-pressure, metallicity and surface brightness. Each bin has about 22 500 counts.

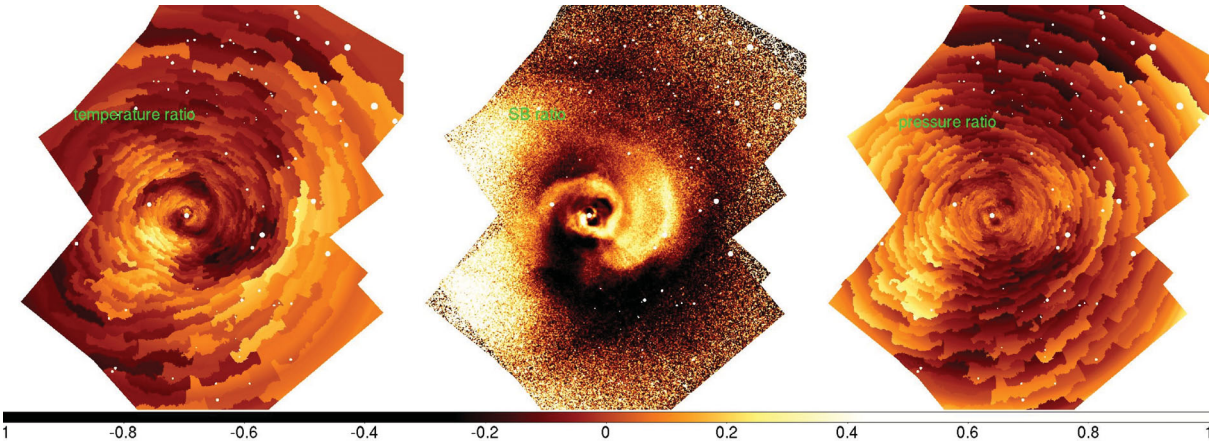

Figure 14. Temperature, surface brightness and pressure distributions. The means at each radius have been subtracted and the intensity is proportional to the fractional difference.

Clearly, these are order of magnitude estimates. By construction they are sensitive only to non-radial part of the substructure and only to the low angular modes. Even more uncertain is the estimate of power (top panel in Fig. 15) which uses the radial sound crossing time as an estimate of the time needed to dissolve the substructure. Nevertheless, taken at face value this figure suggests that the cluster can be broadly divided into two zones at about 100 kpc. (The bright rim to the west of the nucleus is at a radius of ∼110 kpc; see Figs 2 and 6). The estimates of the mechanical power of the central AGN in NGC 1275 give values of order 10^{45} erg s^{-1} over the period of 10^{8} yr (Fabian et al. 2006). If the same estimate is applicable to the mean power during the last Gyr, then the central AGN is not capable of producing the asymmetry outside the central ∼100 kpc region. Instead, the most promising explanation for the substructure beyond 100 kpc is the merger of the Perseus cluster with smaller galaxies/group along the chain of bright galaxies to the west of the core. At yet larger radii beyond 1 Mpc and out to the virial radius, the intracluster gas appears to become intrinsically clumpy (Simionescu et al. 2011).

7 SUMMARY

Our wider image has revealed several structures consisting of dips in surface brightness along the NNW–SSE axis which are plausibly outer rising bubbles. The two new ones are not much larger in pressure-corrected volume than the inner bubbles, whereas the large trough to the north is an order of magnitude larger. Bubbles must be long-lived and we suggest that they may grow in size by merger with other, slower, rising bubbles.

A roughly semicircular cold front is seen to the west of the nucleus of NGC 1275. The metallicity of the gas drops abruptly across the front.

We suspect that the trough and a bay to the south are where rising bubbles have accumulated. The southern bay is distinctly hotter than its surroundings, so the relativistic plasma may have mixed with the intracluster gas there, unlike the situation of the north or the inner bubbles. Both the northern trough and the southern bay lie along a continuation of the west cold front. The other structures seen at radii of 100–150 kpc are likely associated with a subcluster merger (Churazov et al. 2003). The merger also accounts for the east–west asymmetry in surface brightness across the image (Figs 2, 4 and 14).

The energy in substructure peaks at small radii, where it is dominated by activity induced by the AGN, and at larger radii, where it is dominated by the merger.

ACKNOWLEDGMENTS

We acknowledge financial support from the Royal Society (ACF). JH-L thanks the Cambridge Trusts and the Natural Sciences

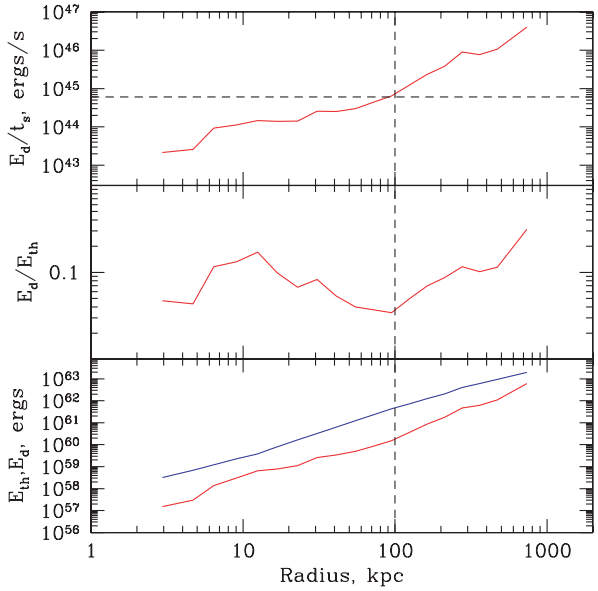

Figure 15. Energy and power associated with non-radial substructure. Bottom panel shows the total ICM thermal energy within given radius $E_{\rm th}(< r)$ (see equation 1) and total energy associated with the observed substructure $E_{\rm d}(< r)$ (equation 2). The ratio of these quantities is plotted in the middle panel. The top panel shows an estimate of power (equation 3) needed to support the observed non-radial substructure. The horizontal dashed line shows an estimate of the central AGN mechanical power, while the vertical line schematically divides the cluster into 'AGN-dominated' and 'merger-dominated' parts.

and Engineering Research Council of Canada (NSERC). GBT acknowledges support provided by the National Aeronautics and Space Administration through Chandra Award Numbers GO0-11139X and GO0-11138B issued by the Chandra X-ray Observatory Center, which is operated by the Smithsonian Astrophysical Observatory for and on behalf of the National Aeronautics Space Administration under contract NAS8-03060. CSR acknowledges support from the Chandra Guest Observer Program under grant GO011138A. SWA was supported in part by the US Department of Energy under contract number DE-AC02-76SF00515. HRR acknowledges generous financial support from the Canadian Space Agency Space Science Enhancement Program.

REFERENCES

Allen S. W., Fabian A. C., Johnstone R. M., Nulsen P. E. J., Edge A. C., 1992, MNRAS, 254, 51
Anders E., Grevesse N., 1989, Geochim. Cosmochim. Acta, 53, 197
Ascasibar Y., Markevitch M., 2006, ApJ, 650, 102
Batchelor G. K., 1987, J. Fluid Mech., 184, 399
Birnboim Y., Keshet U., Hernquist L., 2010, MNRAS, 408, 199
Böhringer H., Voges W., Fabian A. C., Edge A. C., Neumann D. M., 1993, MNRAS, 264, L25
Branduardi-Raymont G., Fabricant D., Feigelson E., Gorenstein P., Grindlay J., Soltan A., Zamorani G., 1981, ApJ, 248, 55
Burns J. O., Sulkanen M. E., Gisler G. R., Perley R. A., 1994, ApJ, 388, L49
Churazov E., Forman W., Jones C., Böhringer H., 2000, A&A, 356, 788
Churazov E., Böhringer H., Kaiser C., Brüggen M., Forman W., 2001, ApJ, 554, 201
Churazov E., Forman W., Jones C., Böhringer H., 2003, ApJ, 590, 225
Conselice C. J., Gallagher J. S., Wyse R. F. G., 2001, AJ, 122, 2281
Diehl S., Li H., Fryer C. L., Raffert D., 2008, ApJ, 687, 173
Dunn R. J. H., Fabian A. C., Sanders J. S., 2006, MNRAS, 366, 758
Fabian A. C., Culhane J. L., Hawkins F. J., Peacock A., Pounds K. A., Parkinson J. H., 1974, ApJ, 189, L59
Fabian A. C., Hu E. M., Cowie L. L., Grindlay J., 1981, ApJ, 248, 47
Fabian A. C. et al., 2000, MNRAS, 318, L65
Fabian A. C., Sanders J. S., Allen S. W., Crawford C. S., Iwasawa K., Johnstone R. M., Schmidt R. W., 2003a, MNRAS, 344, L43
Fabian A. C., Sanders J. S., Crawford C. S., Conselice C. J., Gallagher J. S., Wyse R. F. G., 2003b, MNRAS, 344, 48
Fabian A. C., Sanders J. S., Taylor G. B., Allen S. W., Crawford C. S., Johnstone R. M., Iwasawa K., 2006, MNRAS, 1366, 417
Fabian A. C., Johnstone R. M., Sanders J. S., Crawford C. S., Conselice C. J., Gallagher J. S., Zweibel E., 2008, Nat, 454, 968
Ferrari C., Govoni F., Schindler S., Bykov A. M., Rephaeli Y., 2008, Space Sci. Rev., 134, 93
Forman W., Kellogg E., Gursky H., Tananbaum H., Giacconi R., 1972, ApJ, 178, 309
Gitti M., Brunetti G., Feretti L., Setti G., 2004, A&A, 417, 1
Hatch N. A., Crawford C. S., Johnstone R. M., Fabian A. C., 2006, MNRAS, 367, 433
Heinz S., Brüggen M., Morsony B., 2010, ApJ, 708, 462
Keshet U., Markevitch M., Birnboim Y., Loeb A., 2010, ApJ, 719, L74
Liu W., Li H., Li S., Scott C., 2008, ApJ, 684, L57
Lynds R., 1970, ApJ, 159, L151
Lyutikov M., 2006, MNRAS, 373, L73
McNamara B., Kayemzadeh F., Rafferty D. A., Bîrzan L., Nulsen P. E. J., Kirkpatrick C. C., Wise M. W., 2009, ApJ, 698, 594
Markevitch M., Vikhlinin A., 2007, Phys. Rep., 443, 1
Mazzotta P., Giacintucci S., 2008, ApJ, 675, 9
Nulsen P. E. J., McNamara B., Wise M. W., David L. P., 2005, ApJ, 625, 620
Pedlar A., Ghataure H. S., Davies R. D., Harrison B. A., Perley R. A., Crane P. C., Unger S. W., 1990, MNRAS, 246, 474
Quataert E., 2008, ApJ, 673, 758
Randall S. et al., 2011, ApJ, 726, 86
Rector T. A., Levay Z. G., Frattare L. M., English J., Pu'uohau-Pummill K., 2007, AJ, 133, 598
Reynolds C. S., McKernan B., Fabian A. C., Stone J. M., Vernaleo J. C., 2005, MNRAS, 357, 242
Roediger E., Brüggen M., Simionescu A., Böhringer H., Churazov E., Forman W. R., 2011, MNRAS, 413, 2057
Salomé P., Combes F., Revaz Y., Downes D., Edge A. C., Fabian A. C., 2011, A&A, 531, 85
Sanders J. S., 2006, MNRAS, 371, 829
Sanders J. S., Fabian A. C., 2007, MNRAS, 381, 1381
Sanders J. S., Fabian A. C., Taylor G. B., 2009, MNRAS, 1449
Santra S., Sanders J. S., Fabian A. C., 2007, MNRAS, 382, 895
Sijbring D., 1993, PhD thesis, Groningen Univ.
Simionescu A. et al., 2011, Sci, 331, 1576
Takahashi T. et al., 2010, Proc. SPIE, 7732, 27
Wise M. W., McNamara B., Nulsen P. E. J., Houck J. C., David L. P., 2007, ApJ, 659, 1153
ZuHone J., Markevitch M., Brunetti G., 2011, preprint (arXiv:1101.4627)

APPENDIX A: TEMPERATURE AND PRESSURE PROFILES

Temperature and pressure profiles about the nucleus in 18° steps anticlockwise from west.

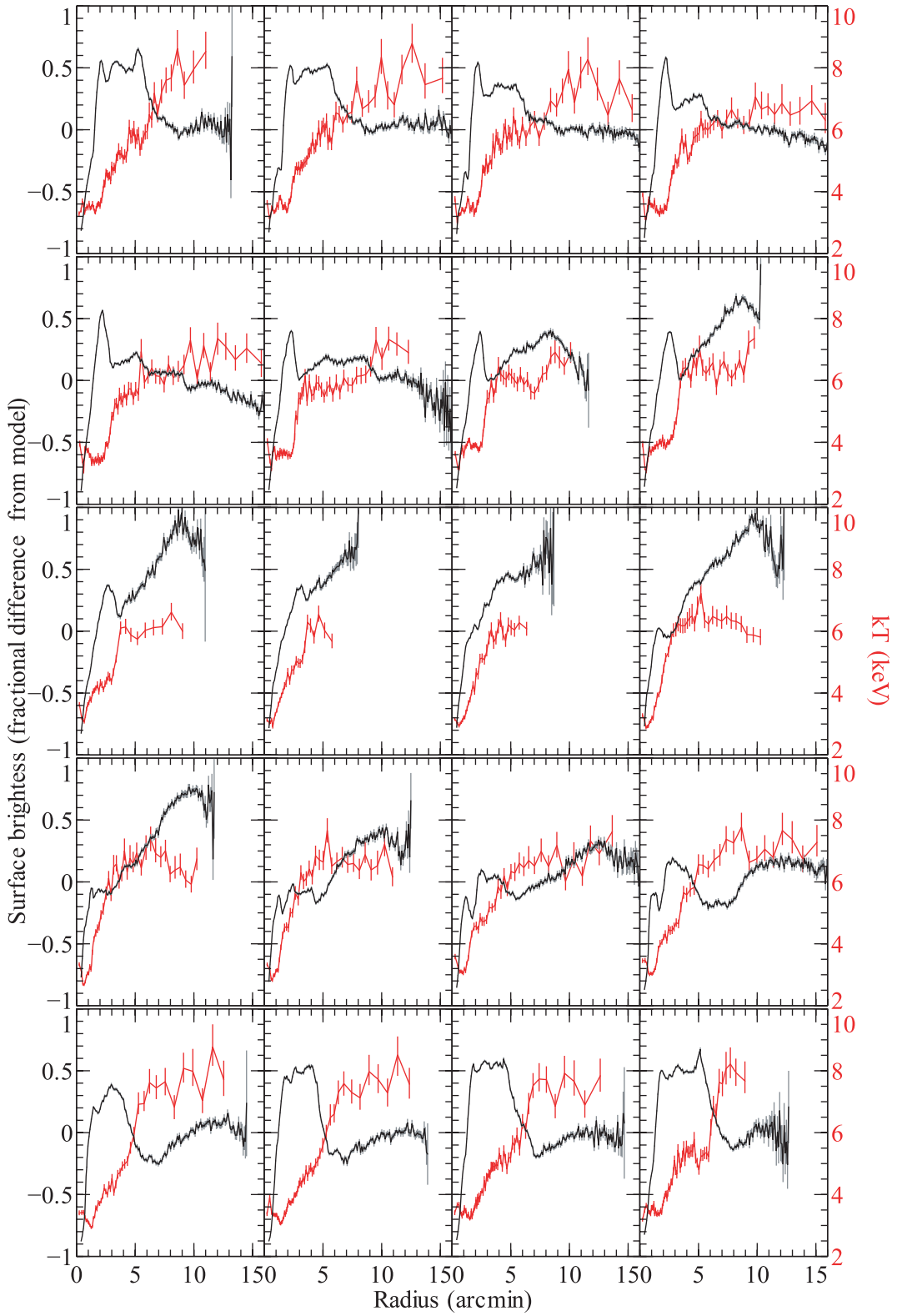

Figure A1. Temperature profiles (in red) with differential surface brightness (black; subtracted from a smooth model) in 20° × 18° sectors arranged from west through north.

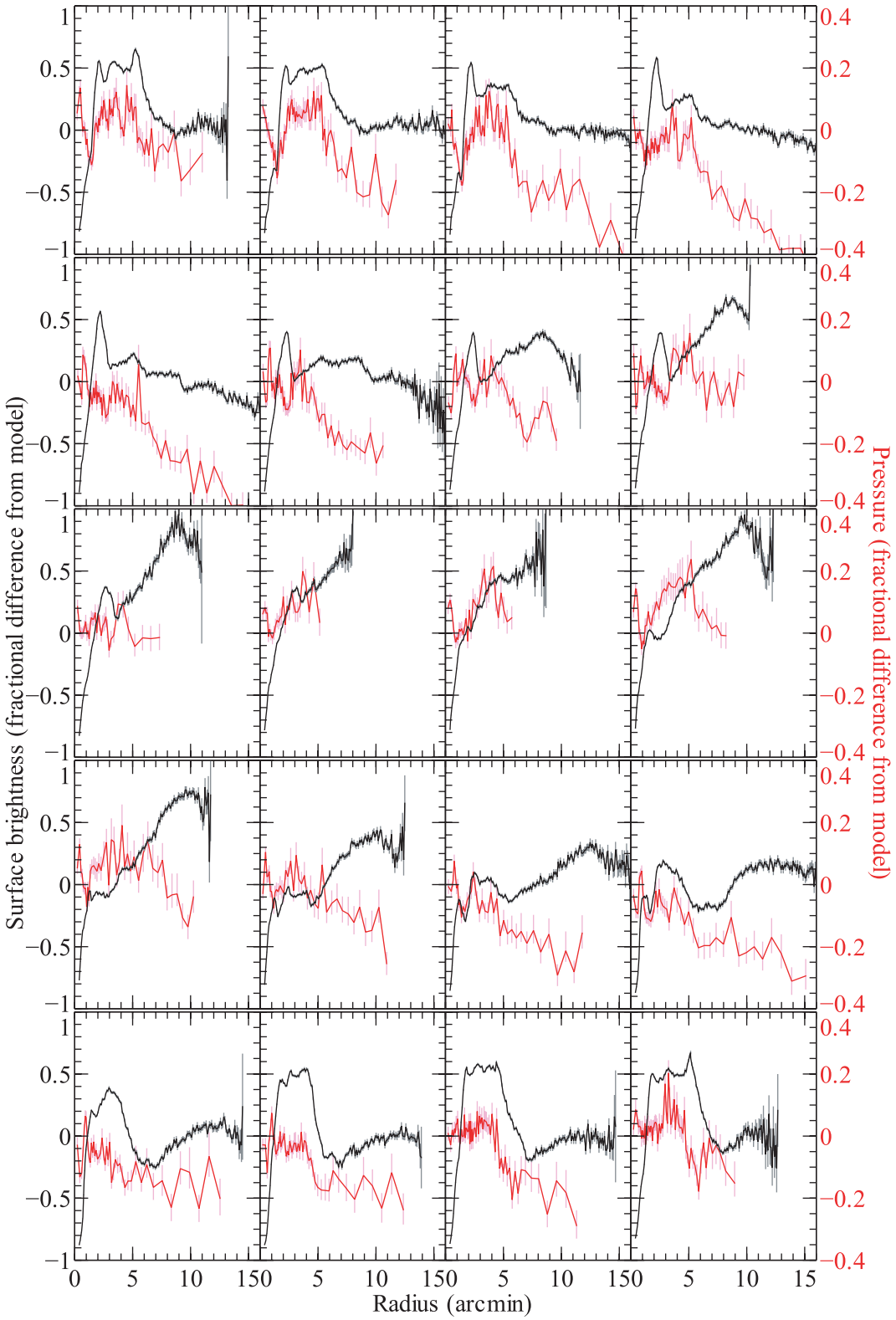

Figure A2. Similar to Fig. 4, but for pressure (the model is a β-profile with a core, which explains why these profiles are somewhat different near the centre from the other profiles, e.g. Fig. 5, which use a power-law model at all radii).

This paper has been typeset from a TEX/LATEX file prepared by the author.